EXAMINING GMI INTERCALIBRATION DEPENDENCE ON THE FULL DYNAMIC RANGE OF BRIGHTNESS TEMPERATURE USING COLD AND WARM END TIE POINTS

John Xun Yang[1,2], Darren S. McKague[1], Christopher S. Ruf[1], Hu Yang[2], Fuzhong Weng[3]

[1]Dept. of Climate and Space Sciences and Engineering, University of Michigan, Ann Arbor, MI, USA
[2]Earth System Science Interdisciplinary Center, University of Maryland, College Park, MD, USA
[3]NOAA Center for Satellite Applications and Research, MD, USA

ABSTRACT

The Earth-scene brightness temperature (TB) seen by satellite radiometers is generally cold over the ocean due to low emissivity, warm over land with high emissivity, and with a large dynamic range dependent on frequency and polarization. Calibration at either cold or warm end cannot fully characterize the calibration dependence on the full TB dynamic range. We have developed calibration methods using both warm and cold reference TB tie points and applied them to the Global Precipitation Measurement (GPM) mission particularly for the GPM Microwave Imager (GMI). The two-end method characterizes the GMI calibration dependence on TB and enables the development of TB-dependent intercalibration correction tables for GPM.

Index Terms—Microwave Radiometry, Calibration, GPM

1. INTRODUCTION

Satellite radiometer calibration is critical for diagnosing instrument performance, correcting hardware issues, and developing science products [1-9]. While most inflight vicarious calibration methods use clear-sky oceanic scenes, they only cover a limited part of the full TB dynamic range. For GMI, TBs at 10 GHz horizontal polarization are 80-100 K over the ocean but 270-290 K over land. Mixed-pixel coastal regions have intermediate TBs. Either cold or warm calibration alone is limited to a narrow range of TBs, which cannot characterize the calibration dependence over the full TB range.

Combining cold and warm calibration supports full-range TB calibration. A radiometer can exhibit calibration errors that are dependent on TB due to hardware issues or improper calibration corrections such as antenna pattern correction (APC) errors [7].

The Intersatellite Radiometer Calibration Working Group (XCAL) members at the University of Michigan (UM) have conducted independent calibration work for GPM. Inspired by previous studies, the cold and warm calibration methods have been independently developed at UM [6-8]. In this study, we combine the cold and warm methods to characterize the GMI calibration dependence on TB.

2. METHODOLOGY

When calibrating a radiometer, a reference independent of the radiometer on-board calibration subsystem is often used to perform vicarious calibration. It can be on-Earth targets with reanalysis data [4, 6], the cosmic background in deep-space maneuvers [9], or a different independent radiometer [3]. We use TMI as a reference radiometer to assess the performance of the target radiometer GMI through intercalibration. We have also done intercalibration between GMI and the other GPM constellation radiometers.

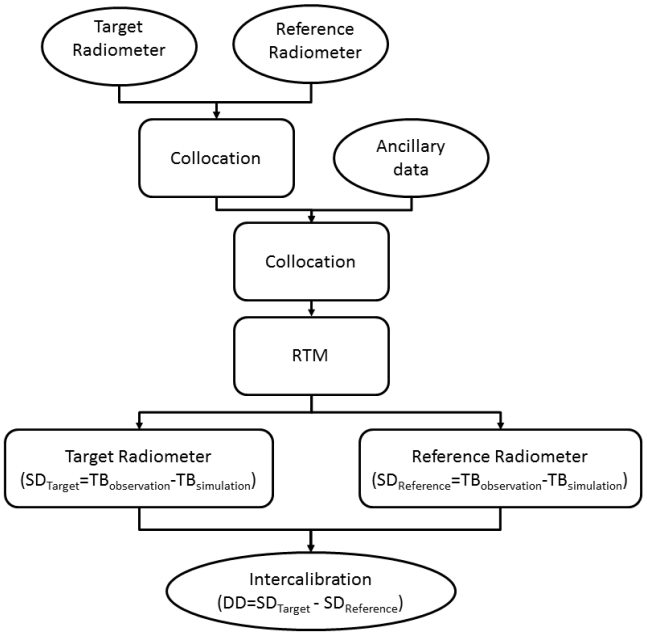

Figure 1. Strategy of radiometer intercalibration, adapted from [8].

The cold and warm calibration methods have been developed at UM, where oceanic scenes are used for cold-end [4] and worldwide forests are used for warm-end calibration [6]. A brief introduction is given here. Figure 1 shows the methodology flowchart. When intercalibrating radiometers, the reference radiometer serves as the transfer standard for the constellation radiometers, while a target radiometer will be calibrated to the reference radiometer.

Within this processing flow, the first collocation is implemented to pull out collocated observations from the reference and target radiometers. After the collocated data between the reference and target radiometers are produced, a second collocation is conducted with ancillary data that provide geophysical fields such as sea surface temperature, surface wind speed, atmospheric humidity, and temperature profiles. The second collocation assigns these geophysical fields to the observed data. We use the National Centers for Environmental Prediction (NCEP) Final (FNL) Tropospheric Analyses data.

A radiative transfer model (RTM) is used to simulate TBs from the ancillary data corresponding to the observed TBs. The RTM is a one dimensional plane-parallel model developed at the UM [8]. Two different surface emissivity models are used for the cold and warm end, respectively.

After implementing the RTM simulations, the difference between the reference and target radiometers can be computed and analyzed. The single difference (SD), observed minus simulated TB, is computed for each individual radiometer. The double difference (DD), i.e., subtracting the single difference for the reference radiometer from that for the target radiometer, is the relative bias of the target to the reference radiometer that accounts for radiometer difference in frequency, EIA, and bandwidth.

3. CALIBRATION DEPENDENCE ON TB

We examine the calibration dependence on TB by combining cold and warm calibrations. The relationship of DD and TB is examined for GMI-TMI intercalibration in subsequent plots. These plots are derived from both cold and warm results. The plots show the 2D number density relationship between DD and TB. A linear regression is performed for each channel as shown in the red line. The scale and offset parameters derived from the linear regression have been used to develop the intercalibration table for GPM.

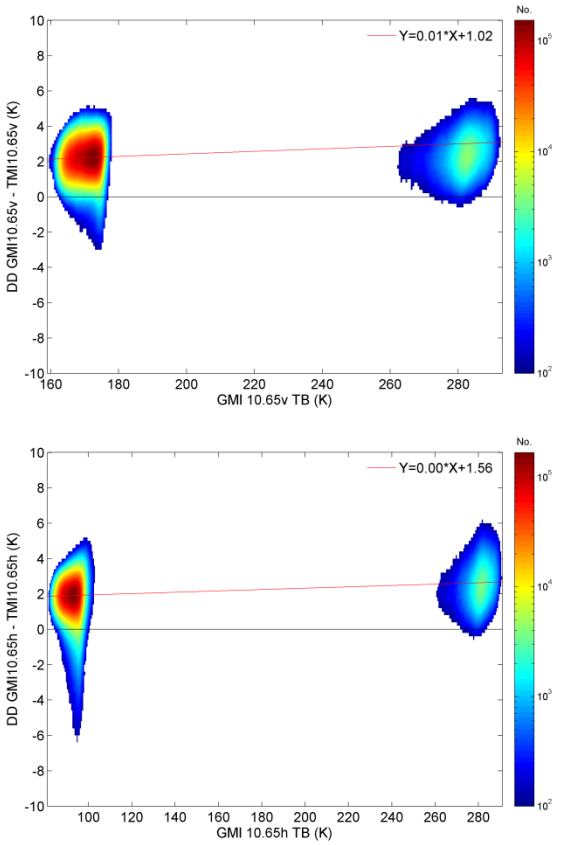

Figure 2. DD Vs TB for GMI-TMI at 10V and 10H respectively.

At channels 10V&H, the cold and warm scenes show clear bimodal structure as shown in Figure 2. That is, cold TBs are around 80K and 170K with warm TBs of 280K for 10V and 10H, respectively. The linear regression shows an increasing trend of DD as a function of TB, which is about 2K-DD per 100K-TB. Although the linear regression does not appear to perfectly represent all the samples, this positive DD-TB trend is appreciable. There is some scatter in the DDs at both cold and warm ends. In particular, the warm-end scattering is relatively significant. This can result from the fact that low-frequency channels have larger field of views (FOVs) than high frequency channels and are therefore vulnerable to surface heterogeneity. The linear regression is used to represent the trend of the DD-TB relationship. It should be pointed out that the lack of middle-range TBs results in difficulty in characterizing the calibration dependence on TB. For instance, the cold and warm modes are separated by ~160 K where nonlinearity could exist. For high-frequency channels, there is no big gap between the cold and warm ends.

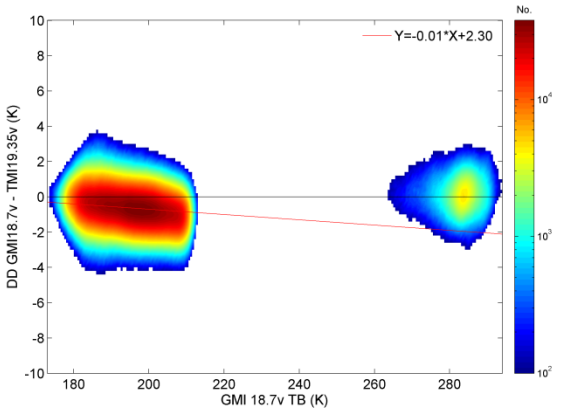

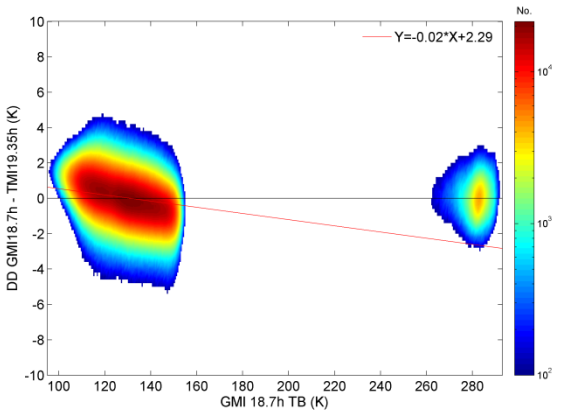

Figure 3: DD Vs TB at 19V and 19H, respectively.

The 19V and 19H channels are shown in Figure 3. Like 10GHz channels, the bimodal TB distribution is significant, though with closer distance between cold and warm ends. The warm-end scattering is reduced compared to 10GHz, since FOVs at 19 GHz are smaller. One very distinct feature is that the linear regression is close to zero. However, the cold-end shows clear decreasing trend with TB. In fact, the cold-end DD decreases with TB by 5K over a 100K change in TB at 19H. GMI and TMI have the same frequency at X-band (10.65 GHz), but differ at K-band with channels at 18.7 and 19.35 GHz respectively. The frequency difference is taken into account by the intercalibration method, but likely has some residual difference due to biases in the frequency dependent model parameterizations.

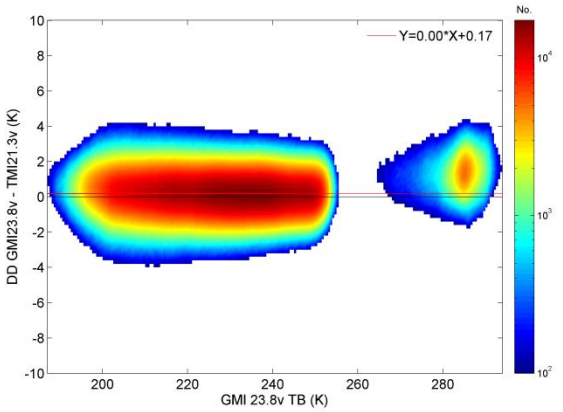

Figure 4: DD Vs TB at 22V.

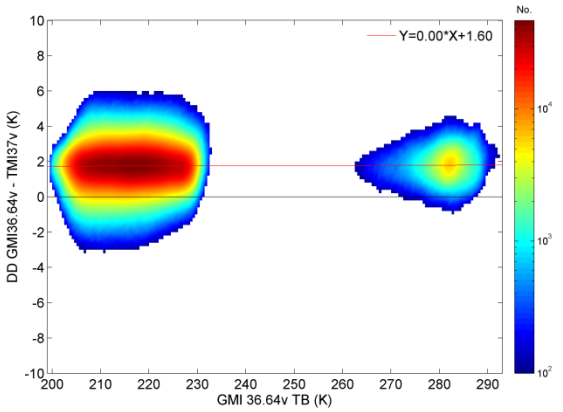

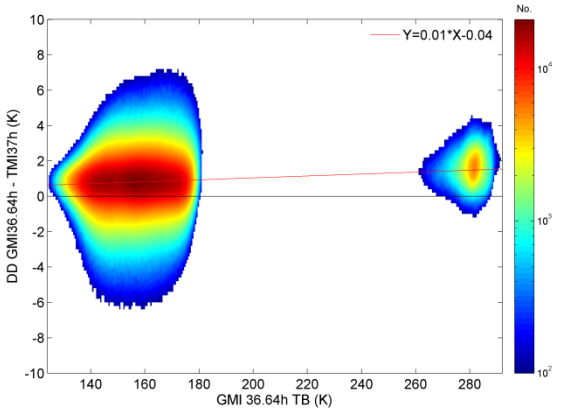

Figure 5: DD Vs TB at 37V and 37H, respectively.

Figure 4 shows the DD vs. TB behavior for the 22V channel. 22V is the water vapor channel and is very warm at the cold end but the bimodal distribution of calibration TBs remains visible. It has a positive slope with 2K-DD per 100K-TB. Channels 37V and 37H are shown in Figure 5. The cold and warm ends are well aligned using the linear regression. The slope is half that of 22V.

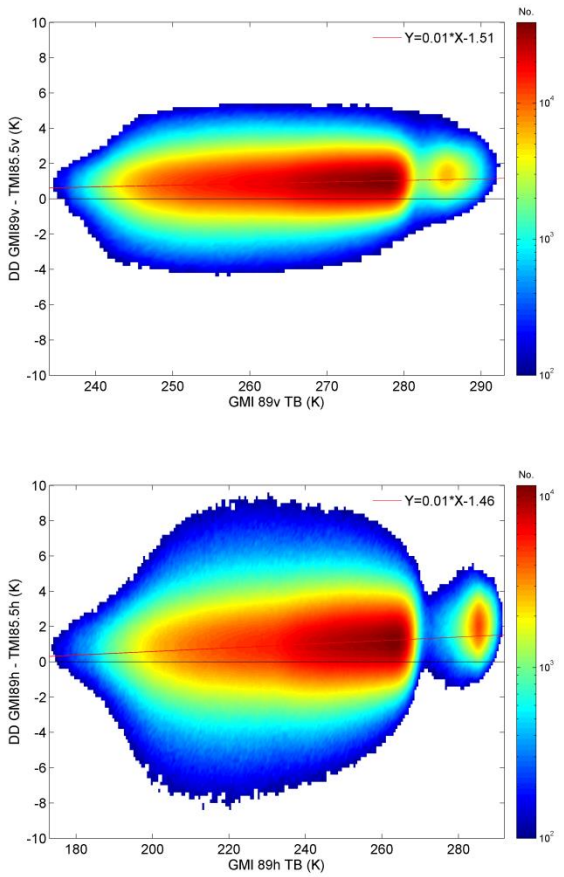

Figure 6: DD Vs TB at 89V and 89H, respectively.

Figure 6 presents results for 89V and 89H. The frequency is high enough that cold-end TBs merge with warm-end. The linear regression well represents a positive trend, where channel 89H has relatively large slope of 6K-DD per 100K-TB. Keep in mind that the range at 89H is small so that the linear regression is sensitive to any uncertainty that would affect intercalibration slope.

4. CONCLUSIONS

Calibration covering the full TB dynamic range has been implemented using the cold and warm calibration methods. This allows the examination of calibration dependence on TB that can be linear or nonlinear. The GPM constellation is intercalibrated and GMI performance is assessed. Linear behavior is found to characterize the TB dependence well. Although the TB dependence varies when intercalibrating different radiometers, the linear behavior generally holds the same. The GPM intercalibration table has been developed using a linear-regression based method as a function of TB to reconcile radiometer differences.

REFERENCES

[1] D. Draper, D. Newell, F. Wentz, S. Krimchansky, and G. Skofronick-Jackson, "The Global Precipitation Measurement (GPM) Microwave Imager (GMI): Instrument Overview and Early On-Orbit Performance," *Selected Topics in Applied Earth Observations and Remote Sensing, IEEE Journal of,* vol. PP, pp. 1-11, 2015.

[2] A. Y. Hou, R. K. Kakar, S. Neeck, A. A. Azarbarzin, C. D. Kummerow, M. Kojima, R. Oki, K. Nakamura, and T. Iguchi, "The Global Precipitation Measurement Mission," *Bulletin of the American Meteorological Society,* vol. 95, pp. 701-722, 2014/05/01 2013.

[3] T. T. Wilheit, "Comparing Calibrations of Similar Conically Scanning Window-Channel Microwave Radiometers," *IEEE Trans. Geosci. Remote Sensing,* vol. 51, pp. 1453-1464, Mar 2013.

[4] J. X. Yang and D. S. McKague, "Improving Collocation-Based Scan Dependent Intercalibration over the Ocean for Spaceborne Radiometry," *IEEE Geoscience and Remote Sensing Letters,*13 (4), 589-593, 2016.

[5] J. X. Yang, D. S. McKague, and C. S. Ruf, "Land Contamination Correction for Passive Microwave Radiometer Data: Demonstration of Wind Retrieval in the Great Lakes Using SSM/I," *Journal of Atmospheric and Oceanic Technology,* vol. 31, pp. 2094-2113, Oct 2014.

[6] J. X. Yang, D. S. McKague, and C. S. Ruf, "Boreal, Temperate, and Tropical Forests as Vicarious Calibration Sites for Spaceborne Microwave Radiometry," 54 (2), 1035-1051, *IEEE Trans. Geosci. Remote Sensing,* 2015.

[7] J. X. Yang, D. S. McKague, and C. S. Ruf, "Identifying and resolving a calibration issue with GMI," *2015 IEEE International Geoscience and Remote Sensing Symposium (IGARSS),* 2015.

[8] J. X. Yang, "Spaceborne Microwave Radiometry: Calibration, Intercalibration, and Science Applications," Doctoral Dissertation, University of Michigan, Ann Arbor, 2016.

[9] F. J. Wentz, P. Ashcroft, and C. Gentemann, "Post-launch calibration of the TRMM microwave imager," *IEEE Trans. Geosci. Remote Sensing,* vol. 39, pp. 415-422, Feb 2001.